Volume 11, Issue 1, January – 2026 International Journal of Innovative Science and Research Technology
ISSN No: -2456-2165 https://doi.org/10.38124/ijisrt/26jan1428

Modeling Ferrite Formation in Mild Steel Weld Using FEM and JMAK Equation

Alain Ngenzi[1]

[1]Pan African University Institute for Basic Sciences, Technology and Innovation (PAUSTI), Nairobi, Kenya

Publication Date: 2026/02/19

Abstract: Having good mechanical properties in the welded steel joint, need to predict accurately the volume fraction of the phase in joint. In hypo-eutectoid steel, to improve the mechanical properties requires determining the kinetics of phase transformation of the austenite to pro-eutectoid steel. This paper proposed a method that can predict the volume fraction of ferrite in mild steel welded joints. To do so, the combination of the finite element method and the JMAK equation was used. TTT diagram and Fe-C equilibrium diagram were considered. The results showed that due to the low carbon content in the steel, the volume fraction of ferrite was determined in the austenite ferrite boundary. The predicted volume fraction was correlated with experimental work documented in the literature.

Keywords: *Finite Element Analysis, JMAK Equation; Volume Fraction of Ferrite; TTT Diagram.*

How to Cite: Alain Ngenzi (2026) Modeling Ferrite Formation in Mild Steel Weld Using FEM and JMAK Equation. *International Journal of Innovative Science and Research Technology*, 11(1), 3628-3636. https://doi.org/10.38124/ijisrt/26jan1428

I. INTRODUCTION

Predictive models have generally been used in various applications to reduce the cost of experimental work. In heating process, predicting the phase change in microstructure has great significance on determine the mechanical properties of the heated materials. Consequently, researchers have been developed different models to predict the phase transformation [1]. Mostly, the phase is formed during the cooling time in many steels, from the austenite finish temperature. In low-carbon steel, hypo eutectoid steel, the phases like pro ferrite, pearlite, and even the martensite phase can be formed. The models that can predict the ferrite phase are empirical model, phase field, Monte Carlo model [1]. Based on the review done by Liu et al. [1], the semi empirical model has shown to fit well with determining the volume fraction of phases. The most used semi empirical method is the Johnson-Mehl-Avrami-Kolmogorov (JMAK) equation.

$$F = 1 - \exp(At^B) \quad (1)$$

Where F is the phase transition in time t, A and B are material parameters. This model is used in the isothermal transformation. The JMAK equation was modified to apply on non-isothermal applications, like welding, using the Scheil additivity rule [2].

The modified JMAK has been used differently. The difference was on expression used to determine parameters of the JMAK, shown in Equation 1. Those parameters have been used in different types of steel to determine the volume fraction of phases. Most of time the parameter, B, is taken as constant because it has been shown as temperature independent parameter [3]. The value of B can be determined using the TTT diagram or some authors have experimentally determined. It was written that the value of B for ferrite is between 0.8 to 1.4 [4]. While the remaining parameter, A, depends on the temperature and has been determined using different methods. The parameter A was determined using the chemical composition and the grain size of austenite [5], modified Gaussian function [6], the Gaussian function obtained using mathematical expression considering the austenite grain size [2], and TTT diagram [7].

In the case of the hypo-eutectoid steel, the volume fraction of ferrite has been predicted with different methods. The ferrite volume fraction was predicted by Phadke et al. [8] using the equilibrium diagram, applying the lever rule. This method was defectively deemed to the fact that the volume fraction of ferrite proportionally decreases with temperature under Ac1 [9] [10]. Then, Lee et al. [11] came with another solution by extending the boundary line of austenite/cementite to obtain the 2 pro eutectoid ferrites under Ac1. They found that the volume fraction of ferrite to be under Ac1.

However, using only the Fe-C equilibrium diagram for predicting the volume fraction of ferrite on hypo-eutectoid steel, the volume fraction of ferrite cannot attain unity. Therefore, Zhang et al. [2] predicted the volume fraction of ferrite in plain carbon steel. The JMAK based on the Gaussian

ISSN No: -2456-2165 https://doi.org/10.38124/ijisrt/26jan1428

function and Fe-C equilibrium diagram. Pohjonen et al. [12] coupled finite difference method and JMAK equation based on the equilibrium diagram to predict the proeutectoid ferrite. Hawbolt et al. [3] predicted the volume fraction of ferrite in 1025 Carbon Steel using the temperature obtained from experimental results and JMAK equation based on the TTT diagram and the Fe-C equilibrium diagram. Sinha et al. [13] predicted the volume fraction of proeutectoid ferrite using the finite element method and the Johson-Mehl equation based on the TTT diagram for hypo eutectoid steel. Kumar and Dixit [14] used the finite element method and microstructure model to predict the volume fraction of ferrite in hypo eutectoid steel. In determining the volume fraction of ferrite, they employed the TTT diagram, equilibrium diagram, and the JMAK equation. However, they applied Phadke's theory in the equilibrium diagram [8].

Despite numerous studies that have focused on numerical simulation of microstructure transformation, additional research is required to increase our grasp of finite element method and microstructure based on TTT diagram and equilibrium diagram, applied the Reti's theory [11]. Therefore, this paper focuses on predicting the volume fraction of ferrite in butt welded steel joint. To achieved that the combination of finite element method, TTT diagram, and Fe-C equilibrium diagram was applied in this paper.

II. METHODOLOGY

➢ *Finite Element Analysis*

Thermal simulation of the GMAW welding process requires a three-dimensional modeling approach. In this study, the non-linear finite element capabilities of ANSYS are employed because of their flexibility and effectiveness in generating full-field numerical solutions. A moving heat source, implemented using the APDL command language, is incorporated into the analysis. The subsequent sections outline the procedures followed in the finite element method**.**

- *Governing Equation and Heat Source Model*

To determine the temperature evolution, the authors utilized Fourier's three-dimensional heat conduction equation [15]. This governing partial differential equation accounts for temperature-dependent material properties and is formulated as follows:

$$k\frac{\delta^2 T}{\delta x^2}+k\frac{\delta^2 T}{\delta y^2}+k\frac{\delta^2 T}{\delta z^2}+\frac{\delta Q}{\delta t}=\rho C\frac{\delta T}{\delta t} \quad (2)$$

Equation 2 contains multiple variables and material parameters. In this equation, Qdenotes the volumetric internal heat generation, while Trefers to temperature. The spatial dimensions are described by the coordinates x, y, and z, and $t$represents time. The model also includes several material properties, where $\rho$is the material density, $C$is the specific heat capacity, and $k$denotes the thermal conductivity. Since the electrode travels along a defined path during the welding process, a moving heat source must be considered. Accordingly, a modified Gaussian heat source model is adopted, with its spatial distribution defined by the Gaussian function illustrated in Figure 1, to simulate the thermal history at various locations within the welded region. [16].

$$Q(x,y,t)=\frac{3q}{\pi r_0^2}e^{\left(-3\frac{r^2}{d_0^2}\right)} \quad (3)$$

Qdenotes the rate of heat input. The effective radius of the welding arc is represented by r_0, and the diameter of the welding arc is represented by d_0. r is calculated by:

$$r=(x-x_0)^2+(y-vt-y_0) \quad (4)$$

Where $x_0$and y_0 represent the distance of the heat source from the reference coordinate system's origin along the x- and y-axes, respectively. The welding arc travel speed is given by v, and the travel time is given by t.

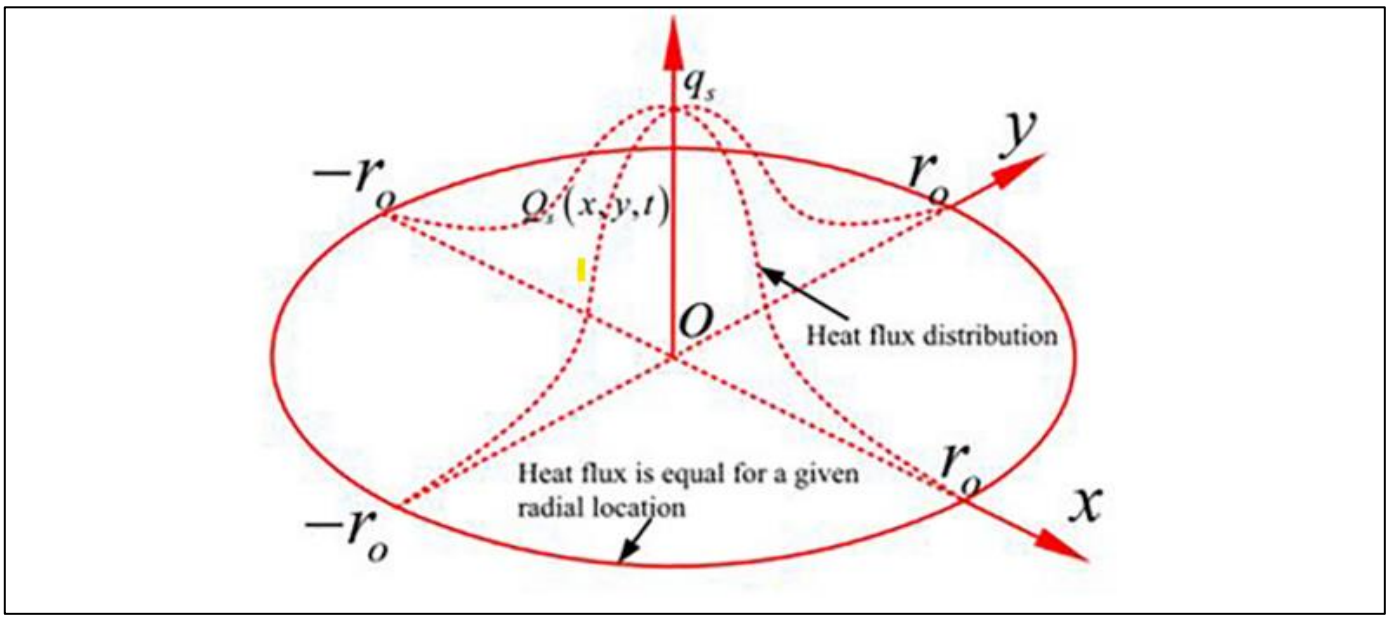

Fig 1 Gaussian Heat Source Model [17]

ISSN No: -2456-2165 https://doi.org/10.38124/ijisrt/26jan1428

- *Mesh*

In this analysis, the geometric model was partitioned into two regions to minimize computational time. Hexahedral elements were employed for discretization. The first region represents the fusion zone and its surrounding area, where elevated temperatures are present, while the second region corresponds to the remaining portion of the model that experiences no significant temperature rise (see Figure 2). The model was discretized into 18,072 elements and 90,730 nodes.

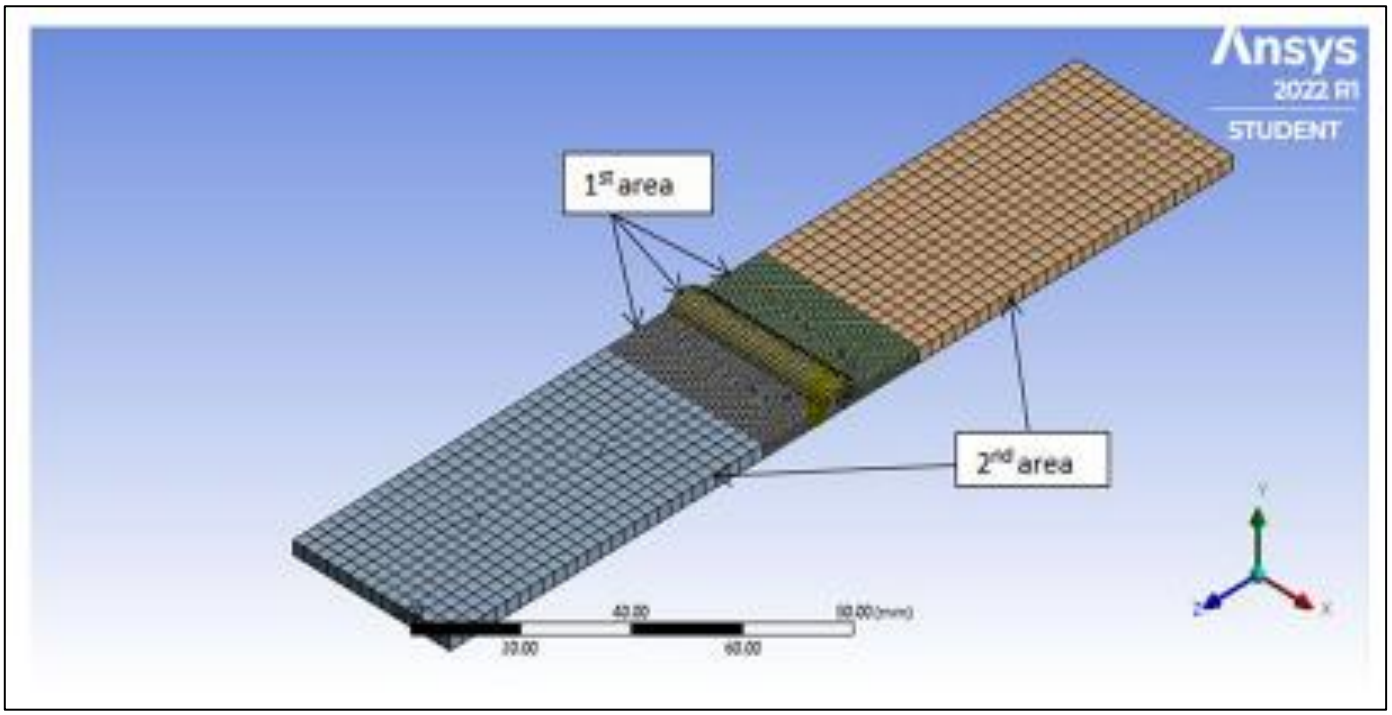

Fig 2 Discretized Geometrical Model

- *Boundary Conditions*

Boundary conditions define the interaction between the computational domain and its surrounding environment. In the welding process, these conditions include an externally applied heat flux on the top surface of the specimen, as well as heat losses caused by radiation and convection acting on all specimen surfaces. Each boundary is represented using appropriate mathematical formulations of thermal boundary conditions. The applied heat flux is modeled using a modified Gaussian heat source, as described in the preceding section. The equation for convection q_c and radiation q_e are written as [18]:

$$q_c = h.(T - T_0) \quad (5)$$

$$q_e = \varepsilon.\xi.(T^4 - T_0^4) \quad (6)$$

The ambient temperature is denoted by T_0, while the convection coefficient and surface emissivity for all plate surfaces are represented by $h$and ε, respectively. The Stefan–Boltzmann constant is indicated by ξ.

- *Material Properties*

In thermal analysis, temperature-dependent material properties play a significant role in governing the temperature distribution during the welding process. These properties include density, thermal conductivity, and specific heat capacity. Since thermal properties vary by material, Table 1 presents the properties of mild steel. The electrode was assumed to have the same thermal properties as mild steel due to the minimal differences in their chemical compositions.

Table 1 Thermal Properties for Mild Steel [19]

T (°C)	Specific Heat (J/kg°C)	Thermal Conductivity (W/m°C)	Density (kg/m³)
0	480	60	7880
100	500	50	7880
200	520	45	7800
400	650	38	7760
600	750	30	7600
800	1000	25	7520
1000	1200	26	7390
1200	1400	28	7300
1400	1600	37	7250
1550	1700	37	7180

ISSN No: -2456-2165 https://doi.org/10.38124/ijisrt/26jan1428

➢ *Ferrite Modeling*

The JMAK equation can be used to predict the volume fraction of ferrite in the low carbon steel. Under isothermal conditions the equation can be written as:

$$F = 1 - \exp(-A(T)t^B) \quad (7)$$

Where F is the phase transition in time t, A and B are material parameters. To determine the values of A and B, the transformation behavior of the material must be studied and quantified using the TTT diagram. For instance, the initial and final volume fractions of phase can be assumed to be F_α=0.01 and F_β=0.99 at the transformation starting and finishing times of α and β on the TTT diagram (see Figure 4). The expressions of those material parameters are written as follows:

$$A = -\frac{\ln(1 - F_\alpha)}{\alpha^B} \quad (8)$$

$$B = \frac{\ln\left[\frac{\ln(1 - F_\alpha)}{\ln(1 - F_\beta)}\right]}{\ln\left(\frac{\alpha}{\beta}\right)} \quad (9)$$

Equation 9 is difficult to use since the TTT diagram for hypo-eutectoid steel, because above eutectoid temperature (Ae1), the ending time of temperature is infinity. This came to consider that the parameter B is constant as was observed by different authors [2, 3, 8]. From that, the value of B (equal to 1) was used in the whole process. This value was taken in literature in which the specimen has same weight percentage of carbon with the specimen used in present research [20]. For the parameter A, a proper TTT diagram for hypo-eutectoid steel was obtained from called JMAT pro software, as shown in Figure 3. In the figure, the different lines showing the start and the finish phase transformation was drawn. The lines were used in determining the different values of starting transformation time at different temperatures. Equation 8 was used to predict the values of parameter A.

Such as welding, where the material is cooled from a high temperature to a low temperature. To describe non-isothermal transformation behavior, a modified approach is needed. One such approach is Sheil's additive rule, which assumes that the overall transformation behavior can be described as a sum of segment of isothermal transformations that occur at different temperatures and times Δt_i during the cooling process (see Fig. 4).

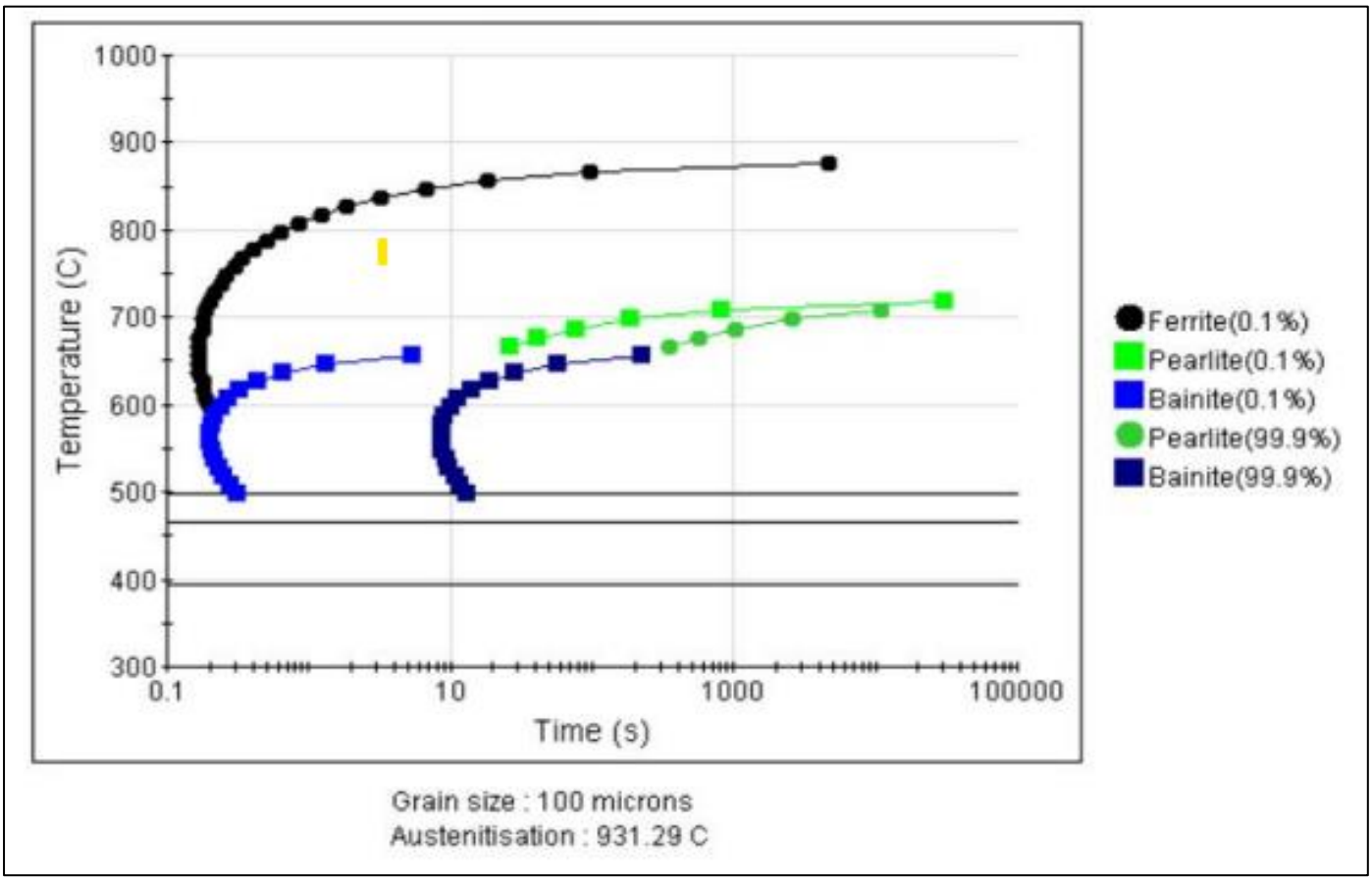

Fig 4 TTT Diagram for AISI 1008 Simulating in JMAT Pro

ISSN No: -2456-2165 https://doi.org/10.38124/ijisrt/26jan1428

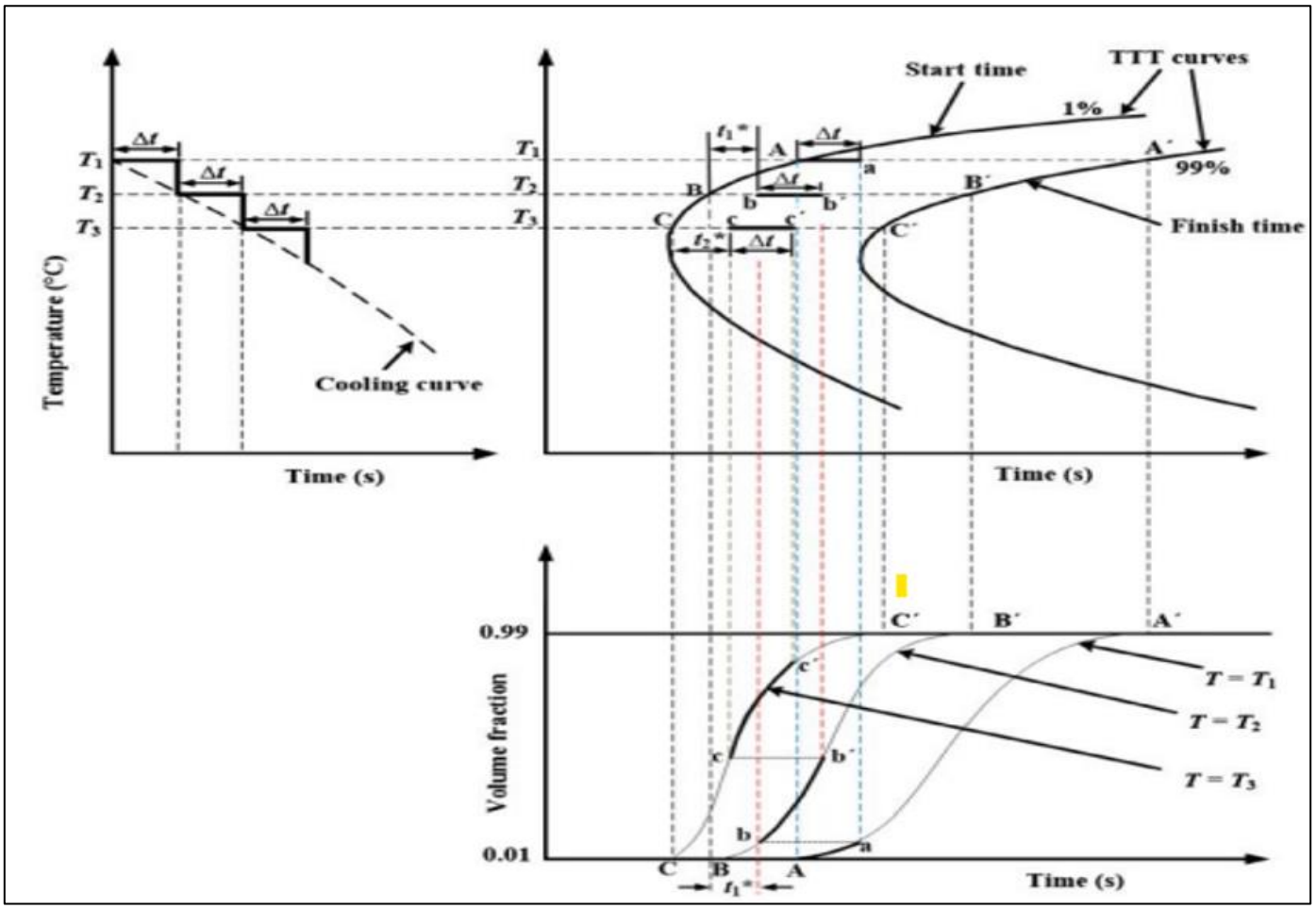

Fig 4 Schematic of Additivity Rule [14]

In the first time segment at temperature T_1, the volume fraction of ferrite transformed after the starting of ferrite transformation can be calculated as follows:

$$X_{F1} = 1 - \exp(-A(T_1)t_1^B) \quad (10)$$

Here, T_1represents the temperature in the first time segment, X_{F1}denotes the ferrite volume fraction at time t_1, and $t_1$corresponds to the initial time increment, which is equal to Δtafter the onset of ferrite transformation. The time increment $\Delta t$is assumed to be 1 s. During the second cooling stage, because each isothermal temperature results in a different ferrite fraction, X_{F1}must be converted to its equivalent fraction, X_{F1}^*, at temperatureT_2.

$$X_{F1}^{'} = \frac{X_{FC}(T_1)}{X_{FC}(T_2)} X_{F1} \quad (11)$$

Where $X_{FC}(T_1)$and $X_{FC}(T_2)$are the equilibrium volume fraction of ferrite at temperatures T_1 and T_1 respectively. Determining the equilibrium volume fraction of ferrite, V_f^{eq}, via Fe-C equlibrium diagram has been applied with various theory. Some tried to use the lever rule combined with densities of austinite, ferrite, and pearlite [2, 3, 8]. However, Lee and Lee [9] provided the simple relation for obtaining V_f^{eq}using the equilibrium diagram. From those two theories, the study used Lee's theory to determine the equilibrium volume fraction of ferrite. The expression is given in Equation 12 and the parameter of the equation is illustrated in Figure 5:

$$V_f^{eq} = \frac{b}{a+b}$$

Or (12)

$$V_f^{eq} = \frac{d}{c+d}$$

Then, the time t_2^* required to produce $X_{F1}^{'}$at T2 can be calculated using the A (T2)
and B:

$$t_2^* = \left[\frac{1}{A} ln\left(\frac{1}{1-X_{F1}^{'}}\right)\right]^{\left\{\frac{1}{B}\right\}} \quad (13)$$

The time segment, Δt, is added to t_2^* for calculating the next volume fraction of ferrite. This procedure is repeated until all the ferrite transformation is finished.

ISSN No: -2456-2165 https://doi.org/10.38124/ijisrt/26jan1428

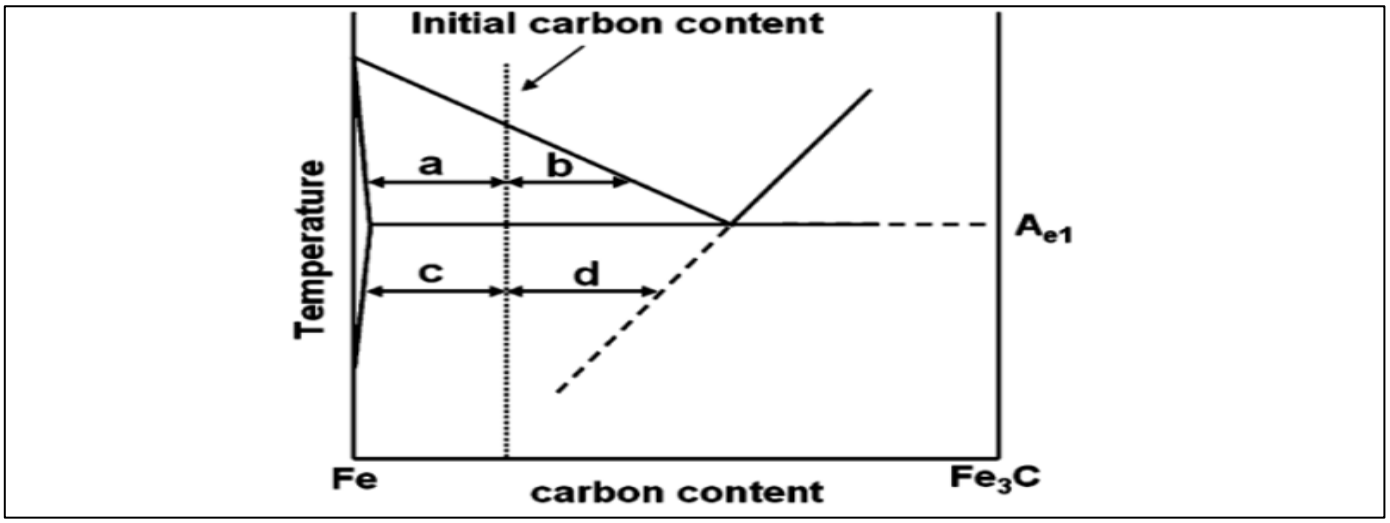

Fig 5 Relation Between the Acm Temperature and the Equilibrium Volume Fraction of Pro-Eutectoid Ferrite by Using a Lever Rule [9].

III. RESULTS AND DISCUSSION

➢ *Mesh*

Owing to the high temperatures experienced in the initial region, a mesh convergence study was conducted using the maximum nodal temperature obtained after simulation as the evaluation criterion. Temperature values were recorded for different mesh sizes. As the mesh was progressively refined, the maximum temperature converged to a stable value, as illustrated in Figure 6. Based on this convergence behaviour, a mesh size of 0.8 mm was selected to minimize computational cost while maintaining accuracy. Consequently, the first region was discretized with a mesh size of 0.8 mm, whereas the remaining region was meshed with a size of 3 mm.

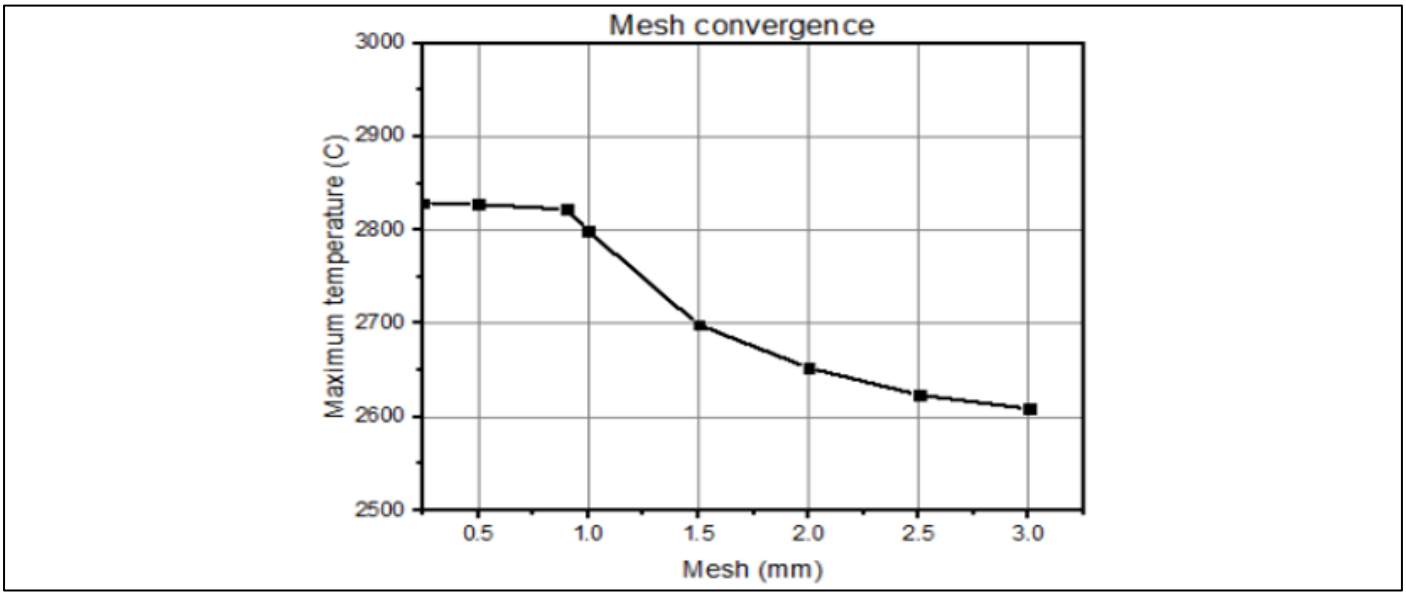

Fig 6 Mesh Convergence

➢ *Temperature History*

The thermal history was evaluated at four distinct locations to examine temperature variations within the welded region. As illustrated in Figure 7, the temperature profiles indicate that the peak temperature exceeds the melting point of mild steel (1430 °C). It is evident that the maximum temperature differs from one location to another, reflecting the movement of the welding heat source and the resulting heat transfer between successive points along the weld path.

This heat transfer is evident from the elevated temperature recorded at the neighbouring node once the preceding node has reached its maximum temperature. Moreover, the adjacent node attains a higher peak temperature than the previous node, indicating progressive heat accumulation.

ISSN No: -2456-2165 https://doi.org/10.38124/ijisrt/26jan1428

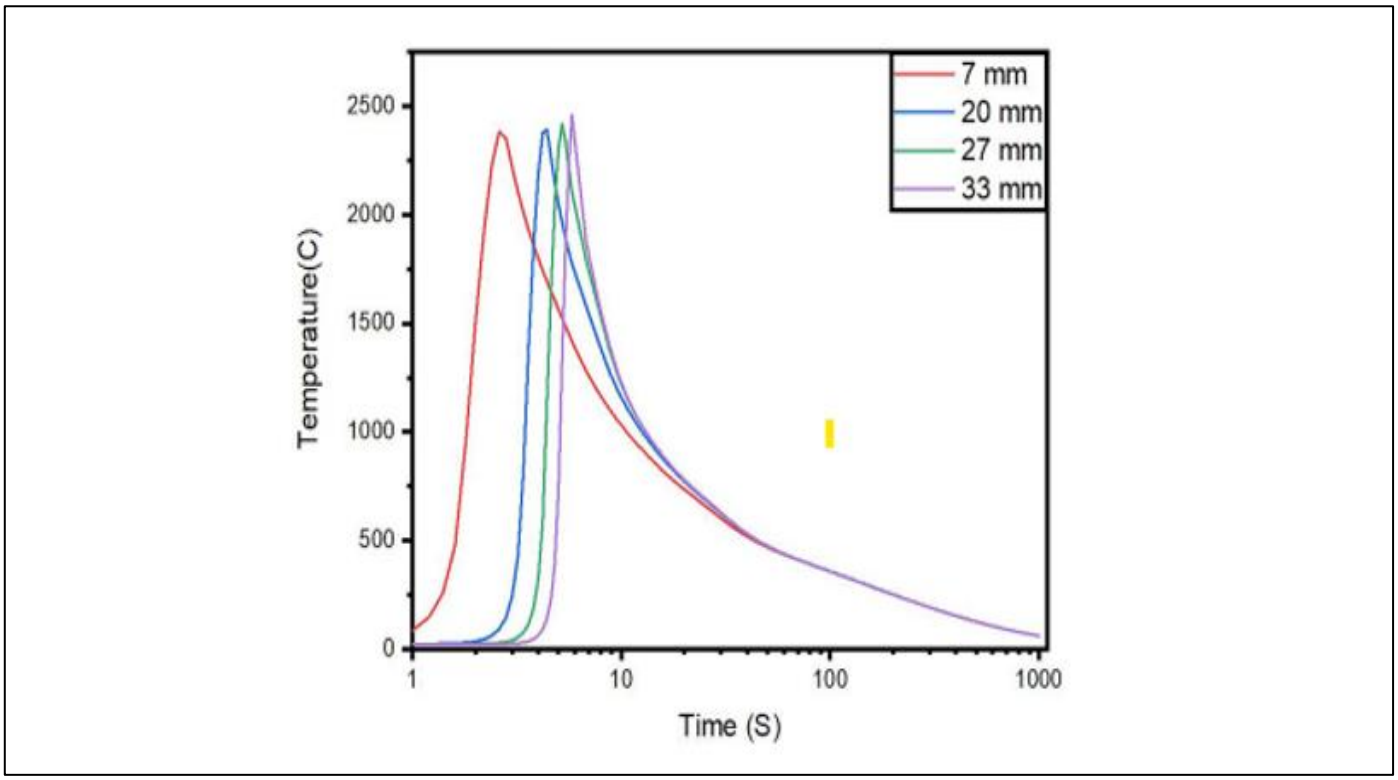

Fig 7 Temperature History at Different Points Along Welded Zone

➢ *Volume Fraction of Ferrite*

The section was concentrated on the prediction of the volume fraction of ferrite in welded mild steel joint. It was stated that the course of the values of parameter A had to be as the C shape [7], as shown in Figure 8. The variation of volume fraction at each step was determined, as shown in Figure 9. In this figure, it can be seen that a small volume fraction was obtained under eutectoid temperature. This was due to the low quantity of carbon present in the hypo-eutectoid steel. It was found that the final volume fraction is 99.8 %. Compare to the experimental work done by Odiaka et al. [21], the obtained result correlated with the experimental result, as shown in Table 2.

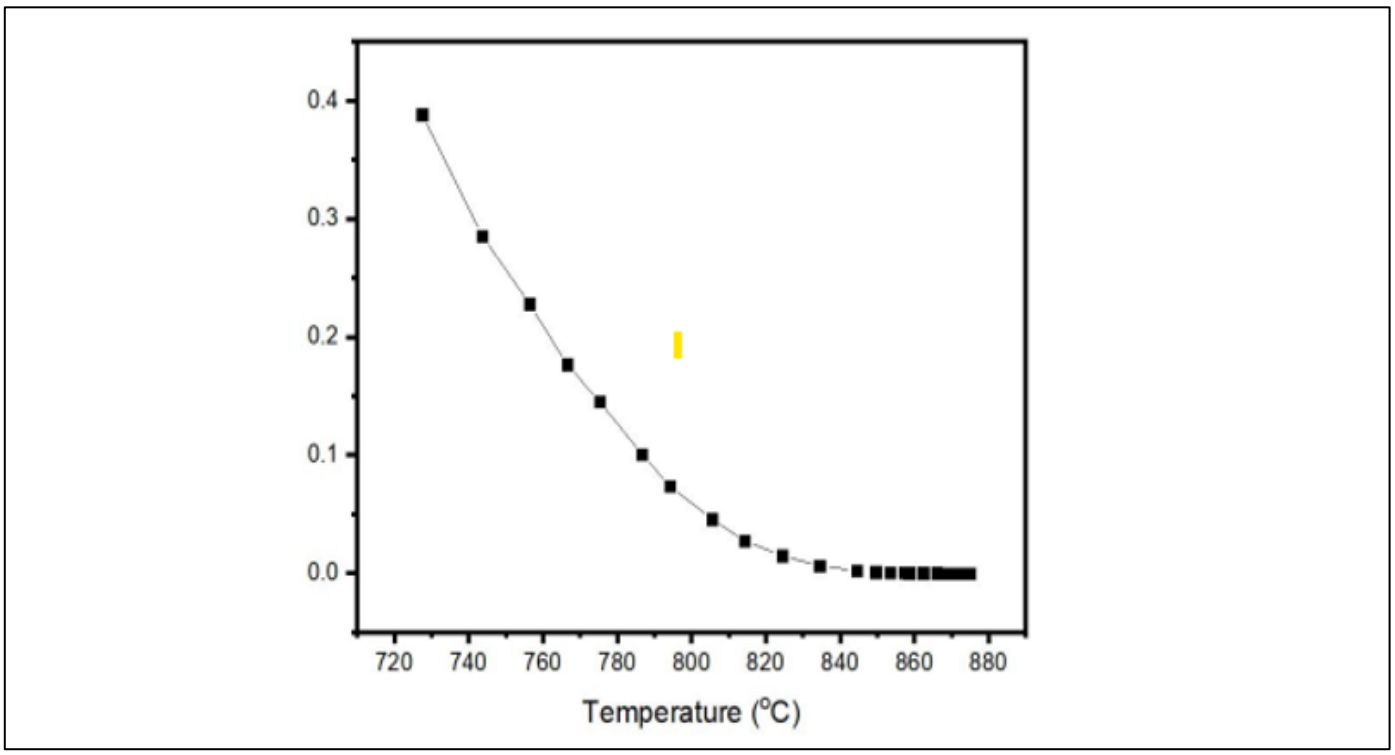

Fig 8 Evolution of Parameter A for JMAK Equation

ISSN No: -2456-2165 https://doi.org/10.38124/ijisrt/26jan1428

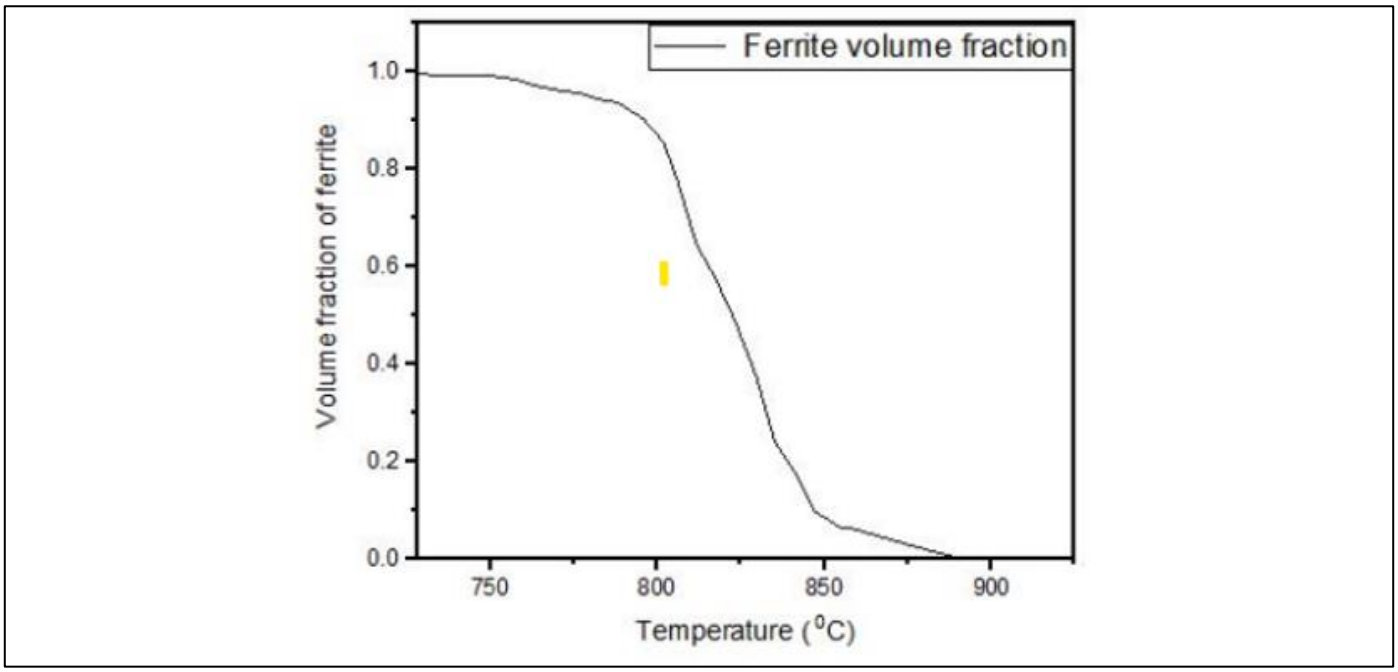

Fig 9 Evolution of Ferrite Phase

Table 2 Comparison of Experimental and Simulation Work

Vol%	
Experimental result	**Simulation result**
100	99.8

IV. CONCLUSION

The volume fraction of ferrite was predicted in this analysis. The combination of finite element method for predicting the thermal history and non-isothermal JMAK equations was adopted. The parameters of non-isothermal JMAK equation were also calculated using Fe-C equilibrium diagram and TTT diagram. A small volume fraction was observed below the eutectoid temperature, which was attributed to the low carbon content in the hypo-eutectoid steel. Simulated results were correlated with experimental work.

REFERENCES

[1]. X. a. L. H. a. Z. M. Liu, "A review on the modeling and simulations of solid-state diffusional phase transformations in metals and alloys," Manufacturing Review, vol. 5, p. 10, 2018.

[2]. Y.-T. a. L. D.-Z. a. L. Y.-Y. Zhang, "Modeling of austenite decomposition in plain carbon steels during hot rolling," Journal of Materials Processing Technology, vol. 171, pp. 175--179, 2006.

[3]. E. a. C. B. a. B. J. Hawbolt, "Kinetics of austenite-ferrite and austenite-pearlite transformations in a 1025 carbon steel," Metallurgical Transactions A, pp. 565--578, 1985.

[4]. M. Militzer, "Computer simulation of microstructure evolution in low carbon sheet steels," ISIJ international, vol. 47, no. 1, pp. 1--15, 2007.

[5]. S. a. H. H. a. J. L. a. Y. J. CG, "A finite element model for the prediction of thermal and metallurgical behavior of strip on run-out-table in hot rolling," ISIJ international, vol. 42, no. 4, pp. 392--400, 2002.

[6]. L. a. L. K. a. Z. Y. Wu, "The kinetics of phase transition of austenite to ferrite in medium-carbon microalloy steel," Metals, vol. 11, no. 12, p. 1986, 2021.

[7]. S.-H. a. I. Y.-T. Kang, "Three-dimensional finite-element analysis of the quenching process of plain-carbon steel with phase transformation," Metallurgical and Materials Transactions A, vol. 36, no. 9, pp. 2315--2325, 2005.

[8]. S. a. P. P. a. S. R. Phadke, "Computational modeling of phase transformations and mechanical properties during the cooling of hot rolled rod," Journal of materials processing technology, vol. 150, no. 1-2, pp. 107--115, 2004.

[9]. S.-J. a. L. Y.-K. Lee, "Thermodynamic Formula for the Acm temperature of low alloy steels," ISIJ international, vol. 47, no. 5, pp. 769--771, 2007.

[10]. A. K. a. B. M. a. S.-F. S. Esfahani, "A numerical model coupling phase transformation to predict microstructure evolution and residual stress during quenching of 1045 steel," Mathematics and Computers in Simulation, vol. 179, pp. 1--22, 2021.

[11]. S.-J. a. P. E. J. a. V. T. C. J. Lee, "Kinetics modeling of austenite decomposition for an end-quenched 1045 steel," Materials Science and Engineering: A, vol. 527, no. 13--14, pp. 3186--3194, 2010.

[12]. A. a. P. J. a. M. J. a. M. T. a. L. J. a. P. D. Pohjonen, "Computer simulations of austenite decomposition of microalloyed 700 MPa steel during cooling," AIP

ISSN No: -2456-2165 https://doi.org/10.38124/ijisrt/26jan1428

Conference Proceedings, vol. 1960, no. 1, p. 090010, 2018.

[13]. V. a. P. R. a. M. A. a. M. J. Sinha, "A mathematical model to predict microstructure of heat-treated steel," Journal of Materials Engineering and Performance, vol. 16, no. 4, pp. 461--469, 2007.

[14]. V. a. D. U. S. Kumar, "A model for the estimation of hardness of laser bent strips," Optics & Laser Technology, vol. 107, pp. 491--499, 2018.

[15]. X. a. X. N. a. L. D. a. L. G. a. S. G. Chen, "The finite element analysis of austenite decomposition during continuous cooling in 22MnB5 steel," Modelling and Simulation in Materials Science and Engineering, vol. 22, no. 6, p. 065005, 2014.

[16]. T. a. A. S. A. a. M. N. a. F. O. S. a. H. S. a. M. Z. a. A. E. T. Odiaka, "umerical analysis of butt and lap welded titanium reinforced mild steel joints," Materials Today: Proceedings, vol. 44, pp. 1175--1184, 2021.

[17]. J. a. H. J. a. D. J. P. a. Y. Z. a. Z. Y. a. Z. Q. Wang, "Development of a new combined heat source model for welding based on a polynomial curve fit of the experimental fusion line," The International Journal of Advanced Manufacturing Technology, vol. 87, no. 5, pp. 1985--1997, 2016.

[18]. D. a. S. K. a. C. S. a. P. M. S. M. Tailor, "Simulation of temperature field of TIG welding using FDM," ASME Pressure Vessels and Piping Conference, vol. 43697, pp. 515--521, 2009.

[19]. A. a. A. S. A. a. M. A. K. Ngenzi, "Predicting the Volume Fraction of Martensite in Welded Mild Steel Joint Reinforced with Titanium Alloy Powder," Modeling and Numerical Simulation of Material Science, vol. 13, no. 2, pp. 11--27, 2023.

[20]. P. a. H. E. a. B. J. Campbell, "Microstructural engineering applied to the controlled cooling of steel wire rod: Part II. Microstructural evolution and mechanical properties correlations," Metallurgical Transactions A, vol. 22, no. 11, pp. 2779--2790, 1991.

[21]. T. a. A. S. a. M. N. a. H. S. a. A. E. Odiaka, "Effect of titanium alloy powder reinforcement on the mechanical properties and microstructural evolution of GMAW mild steel butt joints," Engineering Solid Mechanics, vol. 9, no. 2, pp. 137--152, 2021.